https://doi.org/10.5194/egusphere-2024-2278
Preprint. Discussion started: 25 October 2024

Automated Rapid Estimation of Flood Depth using Digital Elevation Model and EOS-04 Satellite derived flood inundation

Lakshmi Amani Chimata[1], Suresh Babu Anuvala Setty Venkata[1], Shashi Vardhan Reddy Patlolla[1], Durga Rao Korada Hari Venkata[1], Sreenivas Kandrika[1], Prakash Chauhan[1]

[1]National Remote Sensing Centre (NRSC), Indian Space Research Organization (ISRO), Hyderabad, India

Correspondence to: Lakshmi Amani Chimata (amanichimata@gmail.com)

Abstract. Rapid flood assessment is essential for effective relief, rehabilitation, and flood mitigation strategies. Developing and implementing automated, rapid methods for flood depth and inundation estimation are necessary for near real-time information dissemination. This paper presents an end-to-end, automated process for floodwater delineation and depth estimation using EOS-04 (RISAT-1A) Synthetic Aperture Radar (SAR) images and a Digital Elevation Model (DEM). Flood inundation is estimated using an Automated Tile-based Segmentation technique. Flood depth is estimated by the Trend Surface Analysis (TSA) method, a novel technique that requires only the inundated water layer and DEM, unlike various hydrodynamic models that require extensive data. This method is applied to the most flood-prone areas in the states of Andhra Pradesh, Assam, Bihar, and Uttar Pradesh in India. Water levels estimated at river gauge stations using the TSA technique are validated with real-time field measurements and compared with Floodwater Depth Estimation Tool (FwDET)-derived results. The TSA technique outperforms FwDET, showing lower RMSE values.

Key terms: Automation, Flood inundation, Flood depth

https://doi.org/10.5194/egusphere-2024-2278
Preprint. Discussion started: 25 October 2024

1 Introduction

Floods are frequent natural disasters that can have devastating consequences, including loss of life, destruction of property, and disruption of livelihoods. According to the National Disaster Management Authority (NDMA), India is highly susceptible to floods, with over 40 million hectares out of a total geographical area of 329 million hectares prone to flooding (https://ndma.gov.in/Natural-Hazards/Floods). A satellite-derived flood-affected area atlas (1998-2022) indicates that the flood-affected area in India is 15.8 million hectares, reflecting the impact of significant flood events and cyclones (https://ndma.gov.in/flood-hazard-atlases). However, satellite data may have limitations in capturing other flood-affected regions, such as flash floods of short duration and areas lacking satellite coverage during the flooding period. Certain rivers are critical, including the Brahmaputra and Barak in Assam, the Kosi and Ganga in Bihar, the Ganga and Yamuna in Uttar Pradesh, and the Godavari in Andhra Pradesh. Additionally, states frequently affected by cyclones, such as Odisha, Andhra Pradesh, West Bengal, and Gujarat, have necessitated the preparation of Flood Hazard Zonation Atlases for these states, which account for 10 million hectares of flood-affected areas within these six states alone. This highlights the necessity for real-time flood mapping and monitoring, the adoption of automated techniques for flood mapping, and the generation of spatial flood depth information in these areas.

The use of satellite data and derived flood inundation information is popular for addressing the near real-time mapping and monitoring of flood events (Rizwan Sadiq et al., 2022). and this needs to be performed with a reasonable level of confidence in respect of flood inundation areas, flood depth which are essential in near real-time for enabling efficient relief & rehabilitation activities in the field as the spatial information is aimed in this process In this context, both Optical and Microwave satellite data sets are utilized, with the latter being more frequently used due to its advantage of satellite data acquisition under all weather conditions including rain, clouds, and sunlight, unlike sun-synchronous Optical satellite sensors (Felix Greifeneder et al., 2013). Therefore, space-borne Synthetic Aperture Radar (SAR) systems are preferred for flood monitoring. The techniques for discussing satellite-derived flood inundation mapping, flood depth estimation, and case studies are examined from the literature survey. Further, the review underscores the highlights of these studies, and the present research focuses on using newly launched EOS-4 satellite data to develop methodology and implementation for automated rapid estimation of Flood Inundation Mapping and Flood Depth estimation using the Digital Elevation Model.

SAR data uses unique properties of water to detect water covered areas. Generally, low backscatter measurements are possible in calm, open water surfaces with SAR data (Schlaffer et al., 2014). This property of SAR images makes distinguishing water from surrounding surfaces more effectively, even though visual interpretation helps flood mapping (Pierdicca et al. 2008). A literature survey revealed several articles on using SAR images for flood detection using various methods viz. (i) backscatter value-based thresholding (Boni et al., 2016, Chini et al., 2017, Greifeneder et al., 2014, Manjusree et al., 2012, Marti-Cardona et al., 2013, Martinis et al., 2015a, Martinis et al., 2013, Martinis et al., 2009, Twele et al., 2016), (ii) Interferometric coherence calculation (Chini et al., 2019), (iii) region growing and active contour model (Giustarini et al., 2013, Li et al., 2014, Matgen et al., 2011, Tong et al., 2018), (iv) object-oriented classification (Horritt et al., 2001, Kuenzer et al., 2013b, Mason et al., 2010, Pulvirenti et al., 2011), (iv) fuzzy classification (Martinis et al., 2015a, Twele et al., 2016), and (vi) change detection (Bazi et al., 2005, Giustarini et al., 2013, Martinis et al., 2011, Schlaffer et al., 2015, Shen et al., 2018). Among these methods, thresholding-based methods have been most widely used in the literature in part because they are computationally less time-consuming and meanwhile could yield comparable accuracy to the more complex segmentation approaches (Gstaiger et al., 2012; Kuenzer et al., 2013b). Among backscatter histogram thresholding algorithms, the OTSU method has been widely applied in image segmentation (Otsu 1979; Kittler and Illingworth 1986)). This method can automatically calculate the global threshold based on the criterion of maximum between-class variance and has high classification accuracy for images with a uniform bimodal distribution of gray histogram. However, suppose the

https://doi.org/10.5194/egusphere-2024-2278
Preprint. Discussion started: 25 October 2024

histogram is unimodal or has non-uniform illumination, the traditional OTSU algorithm will fail and favour the class with a significant variance to improve the classification accuracy (Xu, X et al., 2011; Yuan et al., 2015). If the object size is less than 10% of the whole area, the performance of OTSU degrades significantly, and it will not be helpful for water detection methods (Cao et al., 2019).

Francesca et al., (2007) have used the method of dividing the SAR image into an unsupervised split-based approach (SBA) for change detection. This method automatically splits the image into a set of non-overlapping sub-images of user-defined size. Then, the sub-images are sorted according to their probability of containing many changed pixels. Afterward, a subset of splits with a high likelihood of containing changes is selected and analysed. This same change detection technique is applied for flood detection by Bovolo and Bruzzone (2007) to identify tsunami-induced changes in multi-temporal imagery. In view of the above limitation in the OTSU method and with the merits of the change detection method, the present study proposed automated delineation of the flood mapping techniques using a Tile-based Segmentation technique i.e., Otsu's thresholding method along with a change detection approach.

However, there is a limitation to this technique when mapping in hilly areas. In very steep slopes, the hillside may appear completely dark, as no radar signal is returned at all, potentially leading to a false interpretation of water pixels. In addressing this issue, Giacomelli et al., (1995) integrated a SAR image with a digital terrain model and employed a simple technique to exclude this false interpretation by utilizing slope, slope direction, and drainage information. Additionally, the Height Above the Nearest Drainage (HAND) tool has been used to exclude hilly areas, enhancing the efficiency of the extracted water layer output, as demonstrated by Nobre et al., (2011). In this approach, HAND raster values are appropriately classified to eliminate false interpretations in the water layer.

In addition to the availability of flood inundation information in near real-time, it is crucial to have access to spatial flood depth maps for directing rescue and relief operations, pooling necessary resources, determining road closures and accessibility, and conducting post-event analysis (Islam et al., 2001). Flood depth identification during or after flood events is critical for assessing hazard levels and creating risk zone maps, which are essential for post-disaster flood mitigation planning. While direct surveying methods used to determine floodwater depth can be highly accurate, they are often influenced by weather conditions, costly, and may require field crews to obtain authorization to access sensitive flooded areas. In light of this, remote sensing-based techniques and digital elevation models (DEMs) are valuable for estimating flood depth (Ismail Elkhrachy et al., 2022). Various hydrodynamic models such as HEC-RAS, Delft-3D, and LISFLOOD-FP have been developed to simulate water levels and flood depths (Yalcin, 2018; Costabile et al., 2021). However, these models require extensive data inputs, such as rainfall, soil moisture, flood maps, gauge discharge, cross-sections, and other hydrological inputs, which result in significant computational time and resource requirements.

Cohen et al. (2007) developed a floodwater depth calculation model based on high-resolution flood extent and DEM layers, known as the FwDET (Flood Water Depth Estimation Tool). The FwDET model identifies the floodwater elevation for each cell within the flooded domain based on its nearest flood boundary grid cell. While FwDET has been evaluated as one of the more effective tools for estimating flood depth from remote sensing-derived water extent and DEM (Teng et al., 2022), it has inherent limitations. One critical limitation is that FwDET's floodwater depth maps are not continuous, often showing sharp transitions in values, which leads to linear stripes across the flooded domain. Additionally, FwDET's floodwater depth accuracy is poor in the case of active channels (Cohen et al., 2018). To overcome these limitations, this paper introduces a novel method called Trend Surface Analysis (TSA) to improve the accuracy of flood depth estimation. This method requires only a flood extent polygon and a DEM as input. Trend surface analysis has long been used by geographers, geologists, and

https://doi.org/10.5194/egusphere-2024-2278
Preprint. Discussion started: 25 October 2024

ecologists to fit surfaces to data recorded at sample points scattered across a two-dimensional sample space (Chorley et al., 1965).

2. Study Area

The research focused on four significantly flood-affected regions in India's river plains: the Godavari, Brahmaputra, Kosi, and Ganga River basins. Table 1 provides detailed characteristics of flood proneness in these regions, while Figure 1 illustrates a location map and the input EOS-04 satellite images of the study areas.

Table 1: Study Area Locations and its characteristics

S.No	Location (Lat/Lon) -decimal degrees	State -Districts Covered, River Basin	Study Area (Sq.Km)	Characteristics of study area
1	17.4008°N to 17.8592°N and 80.9720°E to 81.6582°E	Andhra Pradesh-Alluri Sitaram Raju district	72km × 50km	Receives maximum rainfall during South West Monsoon. 84% of annual rainfall falls during the period starting in mid-June and ending by mid-October
2	25.9885°N to 26.7132°N and 90.6755°E to91.8661°E	Guwahati and Barpeta areas of Assam State	120km x 80km	The Brahmaputra River, known as, the lifeline of Assam, is one of the largest rivers in the world in terms of discharge
3	25.0975°N to 25.7142°N and 86.2874°E to 87.6618°E	Bhagalpur of Bihar State	138km x 68km	Floods frequently occur in Bihar over the Kosi river basin, hence the Kosi river is known as the “Sorrow of Bihar”. Floods are generally caused by the breach of embankment along the Kosi river owing to intense rainfall during the monsoon season
4	27.0138°N to27.6943°N and 79.1919°E to80.1584°E	Farrukhabad area of Uttar Pradesh	95km x 75km	Vast majority of state lies within the Gangetic Plain. The weather is of tropical monsoon type

https://doi.org/10.5194/egusphere-2024-2278
Preprint. Discussion started: 25 October 2024

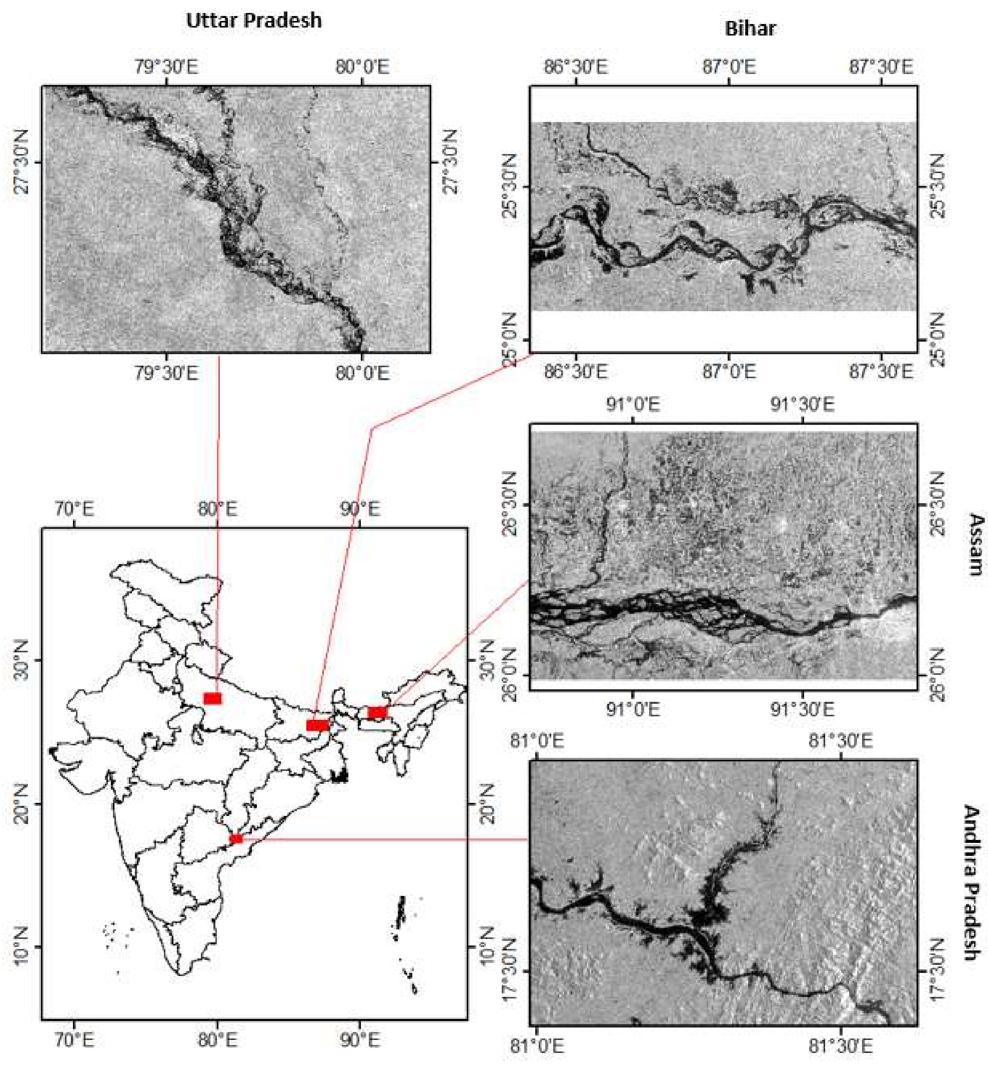

Figure.1. Map showing Four Study Area Locations: Andhra Pradesh, Assam, Bihar and Uttar Pradesh

https://doi.org/10.5194/egusphere-2024-2278
Preprint. Discussion started: 25 October 2024

3. Data used

Table 2 details the information on Satellite data and Digital Elevation Model (DEM) used for deriving Flood inundation and depth estimation. Figure 2 provide the Spatial locations of River gauge stations where field measured water levels are provided by Central Water Commission (CWC) of India.

S.No	Area	Satellite Sensor	Satellite data Spatial Resolution(meters)	Satellite date and Time	DEM	DEM spatial Resolution (meters)
1.	Andhra Pradesh	EOS-04, CRS Mode	36	28th July 2023 at 18:00	LIDAR DEM	5
2.	Assam	EOS-04, CRS Mode	36	20thJune 2023 at 18:00	FAB - DEM COPERNICUS	30
3.	Bihar	EOS-04, MRS Mode	18	3rdSeptember 2023 at 06:00	FAB (Forest and Buildings removed) DEM COPERNICUS	30
4.	Uttar Pradesh	EOS-04, MRS Mode	18	15thAugust 2023 at 06:00	FAB-DEM COPERNICUS	30

Table.2. Satellite data, DEMs used for the study

3.1. Satellite Data digital elevation models

The Earth Observation Satellite-04 (EOS-04) is a synthetic aperture radar (SAR) satellite operating in the C-band frequency range of 5.4 GHz. Positioned in a sun-synchronous orbit at an altitude of 524.87 km, it offers various imaging modes, including Fine Resolution Strip Map Mode-1 (FRS-1), Fine Resolution Strip Map Mode-2 (FRS-2), Medium Resolution ScanSAR Mode (MRS), Coarse Resolution ScanSAR Mode (CRS), and High-Resolution Spotlight Mode (HRS). These modes allow the satellite to capture data with different levels of detail and coverage. The resolution capability of the EOS-04 satellite ranges from 1 m to 50 m, enabling data acquisition at various spatial resolutions.

https://doi.org/10.5194/egusphere-2024-2278
Preprint. Discussion started: 25 October 2024

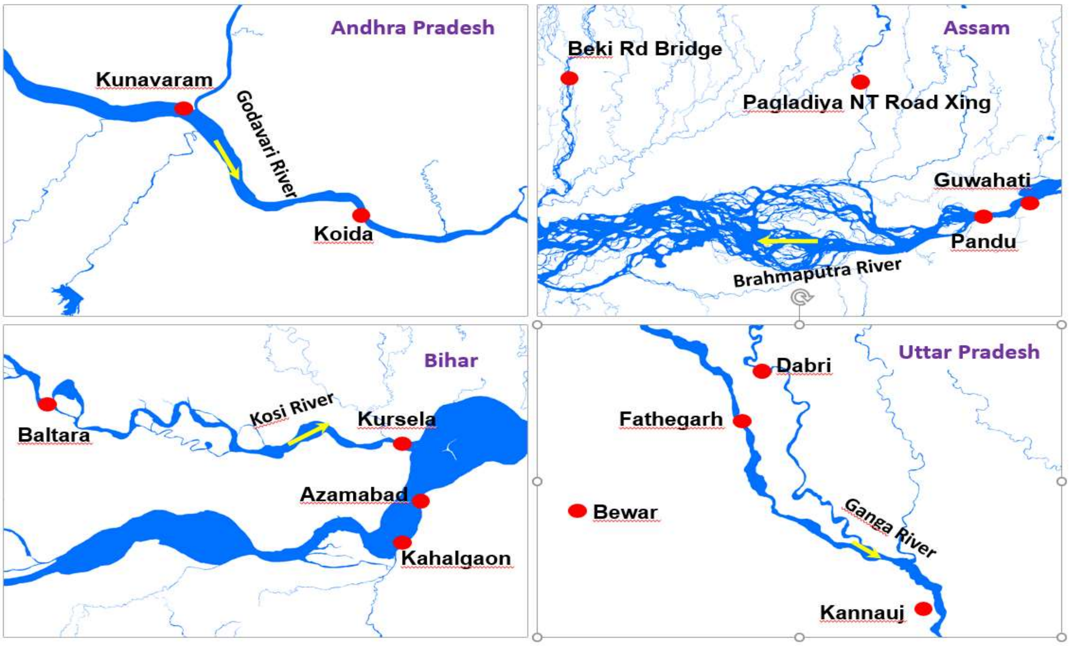

140 **Figure.2.** River gauge station locations at Andhra Pradesh, Assam, Bihar and Uttar Pradesh

3.2. Field Measurements:

Typically, water levels are measured using gauge stations installed along rivers. The Central Water Commission (CWC) of India provides hourly field measurements from these gauge stations, as illustrated in Figure 2, for various sites, and makes the information available on their website (https://ffs.india-water.gov.in/). Water levels recorded at the times corresponding to satellite acquisitions across all study areas are compared with the interpolated levels derived from the Trend Surface Analysis (TSA).

4. Methodology

The process of quickly estimating flood depth using the Digital Elevation Model and EOS-04 satellite involves several steps. These include generating a radar backscatter coefficient image from the raw satellite image, extracting the flood inundation layer using an automated tile-based segmentation method, obtaining terrain information prior to the flood event using digital elevation model, interpolating floodwater surface levels through Trend Surface Analysis, and determining the spatial flood depth. The methodology is illustrated in the flow chart as shown in Figure 3.A customized Python code has been developed specifically for automated flood mapping and depth estimation using ArcGIS and GDAL libraries.

https://doi.org/10.5194/egusphere-2024-2278
Preprint. Discussion started: 25 October 2024

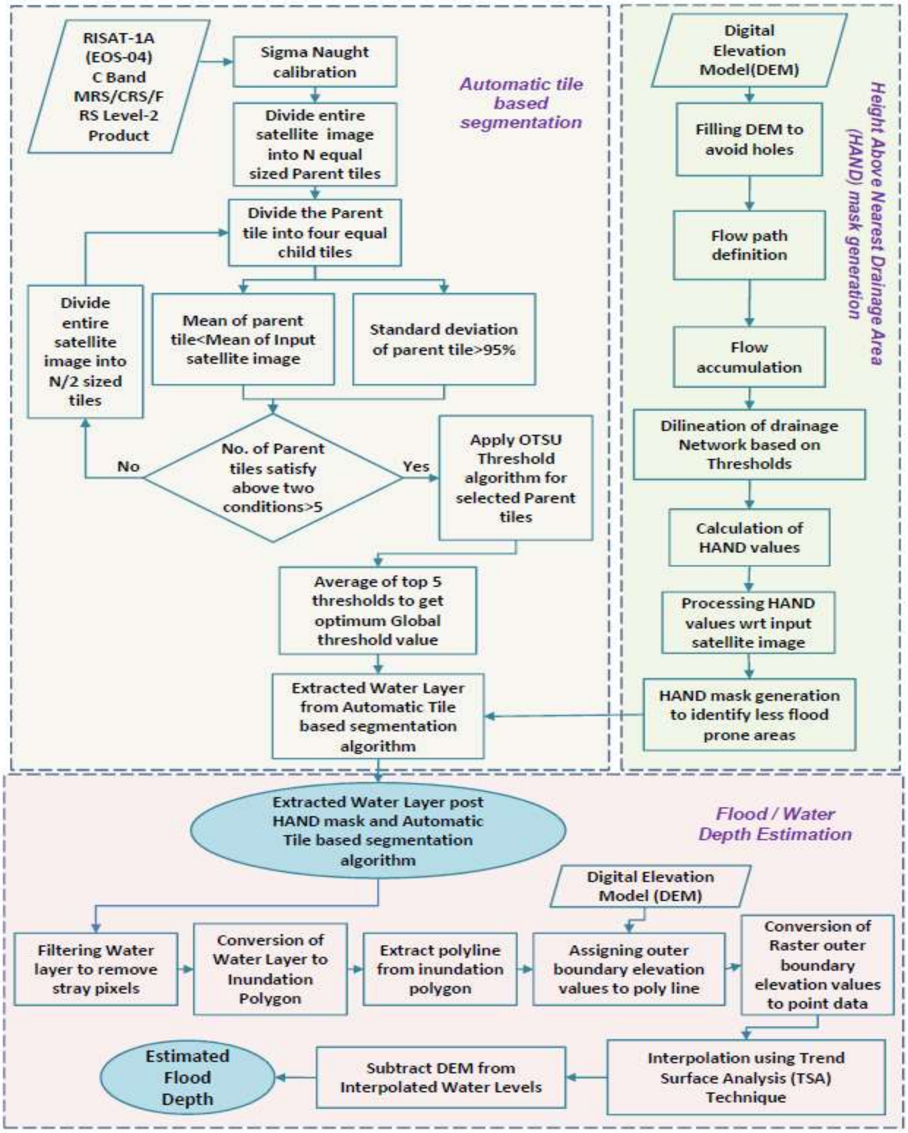

155 **Figure.3.** Flow chart for Methodology

https://doi.org/10.5194/egusphere-2024-2278
Preprint. Discussion started: 25 October 2024

4.1 Generation of radar back scatter coefficient image

Indian Space Research Organisation (ISRO) 's Bhoonidhi portal is a web interface that hosts multi-sensor satellite data. Images acquired from the EOS-04 satellite are directly downloaded from the Bhoonidhi portal. It is necessary to apply radiometric correction to Level 2 product SAR images to truly enable the original Digital Numbers (DN) pixel values to represent the radar backscatter of the reflecting surface. Radiometric correction is essential if one has to compare SAR images acquired with different sensors or acquired from the same sensor at different times, in different modes. Radar backscatter coefficient values, i.e., Sigma Nought (σ_o), are computed as per the following equation:

$$\sigma_o(dB) = 20 * \log_{10}(DN) + 10 * \log_{10} \sin \theta_{inc} - CF$$

where DN represents digital number (amplitude in Level-2 products), $\theta_{inc}$is the per pixel local incidence angle and CF is the Calibration Factor.

4.2 Methodology for Extraction of Flood Layer

The extraction process for the Flood Layer from the Sigma naught calibrated image involves four main steps. These include using an Automatic tile-based segmentation method, obtaining a global threshold value, calculating HAND (Height above the Nearest Drainage Area) mask and extracting the Flood layer.

4.2.1 Automatic Tile Based Classification Method for extraction of Water layer

The Automatic tile-based segmentation method analyses the image in sections called image tiles. This approach divides the entire SAR image into non-overlapping tiles of equal n x n pixels, known as parent tiles. If an equal size partitioning of the image is not feasible, adjustments can be made to the last column and row tiles to ensure that the remaining tiles have equal n x n pixel size. These n-sized parent tiles are further subdivided into 4 equal-sized child tiles. For threshold calculation, certain tiles are selected based on two conditions: (i) the mean individual radar backscatter value of the parent tile should be less than the mean radar backscatter value of the entire SAR image to ensure that the selected tiles are within the SAR image and are located on the boundary between water and non-water areas; and (ii) the standard deviation of the parent tile is greater than 95%, indicating significant variation within the data and leading to a better classification of water and non-water areas. This process is illustrated in Figure 4.

Andrew Twele et al., (2016) analysis shows that if fewer than five percent of parent tiles meet the specified conditions, the SAR image is divided into n/2 x n/2-sized parent tiles. The standard deviation condition for selecting parent tiles can be lowered to 90%, and the process is repeated until the desired condition is met. All the parent tiles that satisfy the above two conditions are subjected to the OTSU threshold technique. The mean of the thresholds is used to calculate the global threshold value for classifying the SAR image. This threshold value helps to distinguish between water and non-water areas.

https://doi.org/10.5194/egusphere-2024-2278
Preprint. Discussion started: 25 October 2024

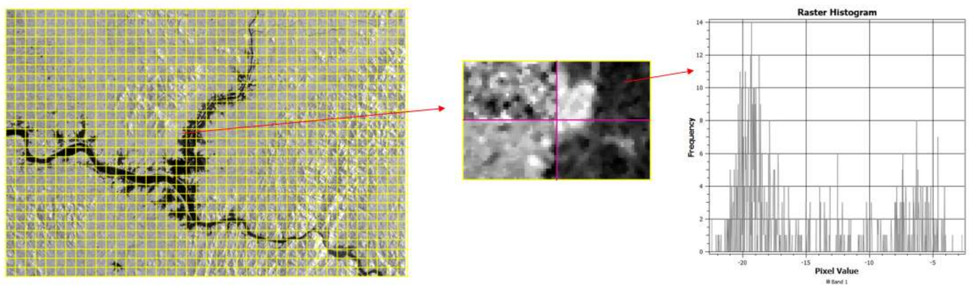

(a) (b) (c)

Figure.4. Automatic Tile based segmentation of SAR image (a)Division of SAR image into n parent tiles (b)Division of parent tile to 4 child tiles (c)Histogram of one child tile

4.2.2. Delineation of Flood layer

It is crucial to ensure that false water areas, such as shadows in steep terrain, are excluded from flood detection. In this context, the filtering process aims to enhance the accuracy of water detection using the Height Above Nearest Drainage (HAND) tool. HAND is a terrain model that standardizes topography relative to the drainage network and is used to characterize local drainage potentials. In a HAND raster, each pixel value represents the vertical distance (in meters) to the nearest drainage channel.

The HAND model leverages DEM inputs to rapidly assess non-flooded areas. Creating a HAND raster image from a DEM involves several steps, as illustrated in Figure 3. These steps include generating a seamless, hydrologically corrected DEM by filling holes, defining flow paths with Flow Direction, identifying the drainage network using Flow Accumulation, and calculating the Height Above Nearest Drainage (HAND) using the D8 flow distance function. The HAND raster provides spatially distributed values that represent the elevation difference between a given point (pixel) and the nearest stream, following the local drainage direction toward the channel where the flow enters

According to Nobre et al. (2015), regions with HAND values greater than 15 exhibit reduced vulnerability to flooding. Consequently, an exclusion mask based on these HAND values is generated for this study. After applying the HAND mask, a suitable water layer is derived using data from the EOS-04 satellite. This water layer undergoes further processing to create a flood map, which overlays the derived water layer with a mask delineating permanent water bodies, such as rivers and lakes.

4.3. Methodology for Flood depth Estimation using Trend Surface Analysis (TSA) Technique

The flood depth in this methodology is estimated by using the inundated water layer and DEM as inputs. First, a water layer is generated polygon using the Automatic Tile-based segmentation method and then converted to polygon. Then, a polyline

https://doi.org/10.5194/egusphere-2024-2278
Preprint. Discussion started: 25 October 2024

is created from the polygon to form the outer boundary segments. This polyline is then converted to a raster. Subsequently, the corresponding outer boundary elevation values from the DEM are assigned to this raster. An interpolation technique is then utilized to estimate water surface elevation values for all the pixels inside the flood boundary. In this paper, we employed the Trend Surface Analysis (TSA) technique for interpolating the elevation values for the entire inundated surface. TSA belongs to the Global Fit interpolation technique, which calculates a single function describing a surface covering the entire map area, as opposed to the Local Fit method which estimates the surface at interpolation points by selecting the nearest data/reference points.

Trend surface analysis is a powerful method that uses global polynomial interpolation to create a smooth surface defined by a mathematical function based on input sample points. This method captures gradual changes and coarse-scale patterns within the data, producing a smooth surface representing the gradual trend across the area of interest. Trend surface analysis involves fitting a polynomial function to known data points and using this function to make predictions for locations where data is not available. The accuracy of the interpolated surface is indicated by the root mean square (RMS) error, with a lower error value signifying a closer representation of the input points. Mathematically, this technique is represented as below:

Observed elevation value at a point on the surface = Predicted Elevation value using TSA method at that point+ residual at that point which is illustrated in following equation

$Z_{observed} = f(x_i, y_i) + r_i (2)$

$Z_{observed}$= The observed elevation value at the ith point

x_i= The coordinate on the X-axis ie Latitude at the ith point

y_i=The coordinate on the Y-axis ie Longitude at the ith point

r_i=residual at the ith point

$f(x_i, y_i)$denote a polynomial function.

Based on the findings of Cohen et al. (2007), Huang et al. (2014), Brown et al. (2016), and Cian et al. (2018), it is assumed that the water surface in flooded areas is flat when calculating flood depth. Since the elevation variations in all four case studies are gradual, this paper utilizes the linear trend interpolation technique for estimating flood depth. The linear trend surface interpolator uses polynomial regression to create a least-squares surface from the input points. This approach allows for customization and flexibility in the analysis process by providing control over the polynomial order used to fit the surface.i.e.

$$f(x_i, y_i) = ax_i + by_i + c$$

where a, b and c are constants

The aim of Trend Surface Analysis (TSA) is to determine the most suitable surface based on outer boundary elevation values, thereby uncovering the fundamental patterns of gradients and contours within the sample space (Morton et al., 1974). In real topographic surfaces, it is unlikely that any observed surface will exactly follow an idealized trend. The observed elevation values will either lie above or below the trend surface, resulting in residuals or prediction errors at each point. A positive residual (above zero) indicates that the trend surface lies below the observed surface at that location, while a

https://doi.org/10.5194/egusphere-2024-2278
Preprint. Discussion started: 25 October 2024

negative residual indicates that the observed surface lies below the predicted trend surface. Each combination of a, b, and c would generate a different inclined plane. Some of these surfaces would be good if the observed points were close to them, resulting in low residual values, whereas other surfaces would be poor if the observed values were distant from them. It would be useful to find a method of determining the very best possible combination of a, b, and c. To choose those constants, the least squares criterion is used, which finds the combination of a, b, and c that minimizes the sum of squares of residuals (S).

$$S = \sum_{i=1}^{N} (r_i^{\,2})$$

Where $r_i = Z_{observed} - (ax_i + by_i + c)$

To estimate flood depth in this paper, the Trend Surface Analysis technique (TSA) is applied to the Water Layer obtained from Automatic flood mapping output. The water layer is converted into a polygon, then into a polyline and a raster. Using the respective DEM, outer boundary elevation values for the water layer are extracted and assigned to the raster. As the TSA technique works only on point data, this raster is converted to point form. Subsequently, the surface is interpolated using the TSA technique based on the flood outer boundary point data. The TSA Interpolated surface provides estimated water levels in meters. Finally, the estimated Flood depth is determined by subtracting the Digital Elevation Model (DEM) from the interpolated water levels. This methodology is further explained in the figure 5.

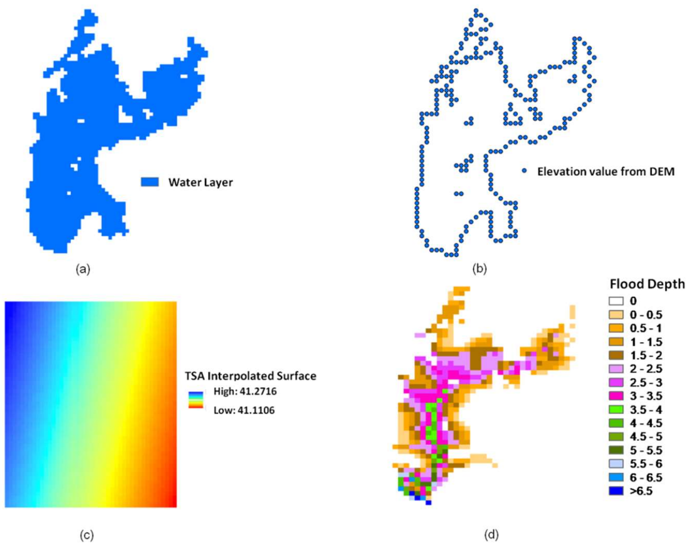

Figure 5: Methodology for flood depth estimation using TSA technique: (a) Water layer created using the Automatic Tile-based segmentation technique. (b) Elevation values extracted from the Digital Elevation Model (DEM) as points.

https://doi.org/10.5194/egusphere-2024-2278
Preprint. Discussion started: 25 October 2024

(c)Interpolated surface is generated using these elevation points through Trend Surface Analysis (TSA).(d)Flood depth is estimated by subtracting DEM values from the interpolated water levels (above mean sea level).

4. Results and Discussion

This research estimates flood inundation areas from SAR image, derives flood boundaries, and simulates flood contours and surfaces based on digital elevation models. The spatial resolution and accuracy of the digital elevation models are crucial for extracting floodwater depth. In this study, a high-resolution LIDAR DEM is used for one case study, the Godavari River reach, while simultaneously using Copernicus FAB 30m DEM to assess the sensitivity of the DEM in determining flood depth. The results from three other study areas Ganga, Brahmaputra, and Kosi rivers are also presented. Additionally, the accuracy of the flood depth values derived from Trend Surface Analysis (TSA) is evaluated by comparing them with field based measured river water levels provided by CWC on that particular day and time. It is also being compared with FWDET Tool.

4.1. Flood Inundation Area Estimation

The flood inundation layer is delineated using the Automatic Tile Based Classification Method on SAR data, with the HAND (Height Above Nearest Drainage) tool applied to eliminate false water areas and accurately identify actual flood water. During the flood disaster, it is challenging to conduct fieldwork for flood map validation. Hence, the accuracy of this delineated flood layer is evaluated using optical satellite cloud freeLandsat-8 image acquired on the same date i.e., 15thAugust 2023 similar to EOS-04 date in the Uttar Pradesh study area. The delineation of water spread in Landsat-8 image is carried out using unsupervised classification techniques using ERDAS imaging software. The results are shown in figure 6.

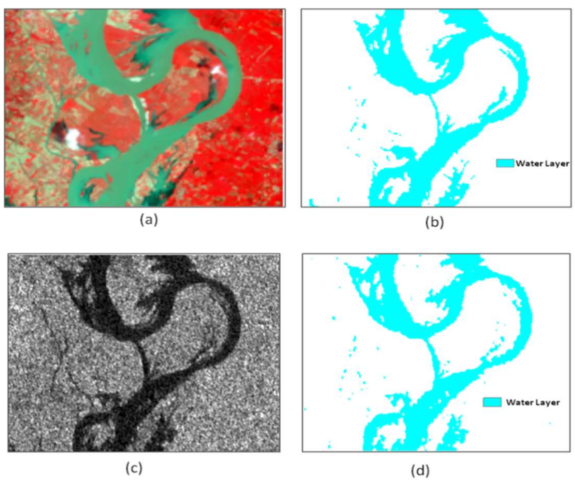

https://doi.org/10.5194/egusphere-2024-2278
Preprint. Discussion started: 25 October 2024

Figure 6: Optical satellite data and EOS-04 data comparison (a) shows the optical Landsat-8 data of Resolution 15m in Uttar Pradesh study area. (b)Water layer extracted from optical data using unsupervised classification. (c) EOS-04 data in the same study area of Landsat-8 data. (d) Water layer extracted from EOS-04 data using Automatic Tile based segmentation algorithm

Area computed	Optical data	SAR data
	446 Ha	455 Ha

Table:3: Statistical area covered under water

As a part of accuracy test, statistical area covered under water delineated from Landsat-8 and EOS-04 image is computed and tabulated in table 3. It is observed that the flood delineation accuracy using Automatic tile-based classification method on SAR data is approximately 94% when compared to optical data. It is also understood from the above figures, that the variation of mismatch is because, in the shallow water areas of flowing waters, microwave data showing as no water which is not true from optical data.

From these results, it is observed that the Automatic Tile Based Segmentation Method is deemed appropriate for deriving flood maps in rapid mode using SAR data. As Flood depth result depends on the delineated flood extent from SAR image, this method is useful for automatic detection of water layer in the SAR image.

4.2. Floodwater Depth Estimation

The shape of flood layers varies across different areas, with some regions appearing wide, indicating a gentle slope, and others being narrow along rivers, suggesting a steeper gradient, as observed in the aforementioned case studies. There is an increasing demand for accurately determining flowing water surfaces to precisely estimate flood depths. Typically, the flowing water surface is derived through two steps: firstly, by collecting elevations along the flood inundation boundary, which represent varying heights of discrete points, and secondly, by fitting a surface across these elevation points using commonly used interpolation methods.

4.2.1. Comparison of DEMs in flood water depth estimation

The accuracy of floodwater depth measurements depends significantly on the accuracy and spatial resolution of the Digital Elevation Model (DEM) as it plays a major role in interpolation of flood water depth. To assess this, an analysis was conducted in the Godavari flood plain area, utilizing two different DEM datasets. One DEM was derived from LiDAR data with a 5-meter spatial resolution and vertical accuracy of 15 cm, while the other was obtained from the public domain, specifically the Copernicus FABDEM, with an 8-meter vertical accuracy and 30-meter spatial resolution. This comparative study aims to evaluate the impact of public domain DEMs on the accuracy of flood water depth estimation. Here, the flood depth is estimated in Godavari Flood plain study area using Trend Surface Analysis (TSA) Technique. The results of this

https://doi.org/10.5194/egusphere-2024-2278
Preprint. Discussion started: 25 October 2024

analysis are presented in the figure 7 below. A scatter plot is drawn for comparison of flood depth values estimated using TSA technique for LIDAR and Copernicus DEMs.

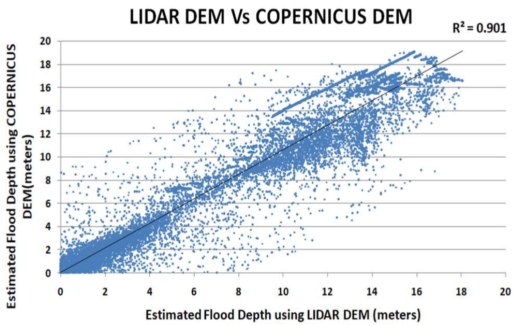

Figure 7: Plot between LIDAR DEM and Copernicus DEM derived Flood depths

The scatter plot above shows that 90% of the flood depth points derived from LiDAR and Copernicus DEMs closely match. Discrepancies predominantly occur in areas with steep slopes where elevation changes rapidly. Therefore, accurate LiDAR-derived DEMs are essential for estimating flood depths in steep areas. In contrast, for areas with gentle slopes, the Copernicus DEM, with its 30-meter spacing provides sufficiently accurate flood depth estimates, as depths are relative to heights.

4.2.2 Derivation of Flood depths using TSA technique in Study Areas

Given the dynamic nature of river elevations and varying water levels at different locations, employing trend surface analysis becomes essential for simulating the flood surface, especially in large flooded areas with gentle slopes. This process involves calculating floodwater depths based on DEM Resolution at specific locations, such as pixels. For Andhra Pradesh study area, LIDAR DEM derived flood water depth using TSA is illustrated in fig 8. For the remaining three study areas such as Bihar, Assam and Uttar Pradesh, publicly available Copernicus DEMs is used to estimate flood water depth using TSA technique. The figure 8 below illustrates the flood depths in four areas of gentle slope. Figure 8(e) represents the legend followed in the flood depth estimation (in meters) in all the four study areas.

From Figures 8(a), 8(b), 8(c), and 8(d), it is evident that the flood depth is greater in river areas and it is represented in blue colour. Flood depths derived from TSA technique are smooth and continuous.

https://doi.org/10.5194/egusphere-2024-2278
Preprint. Discussion started: 25 October 2024

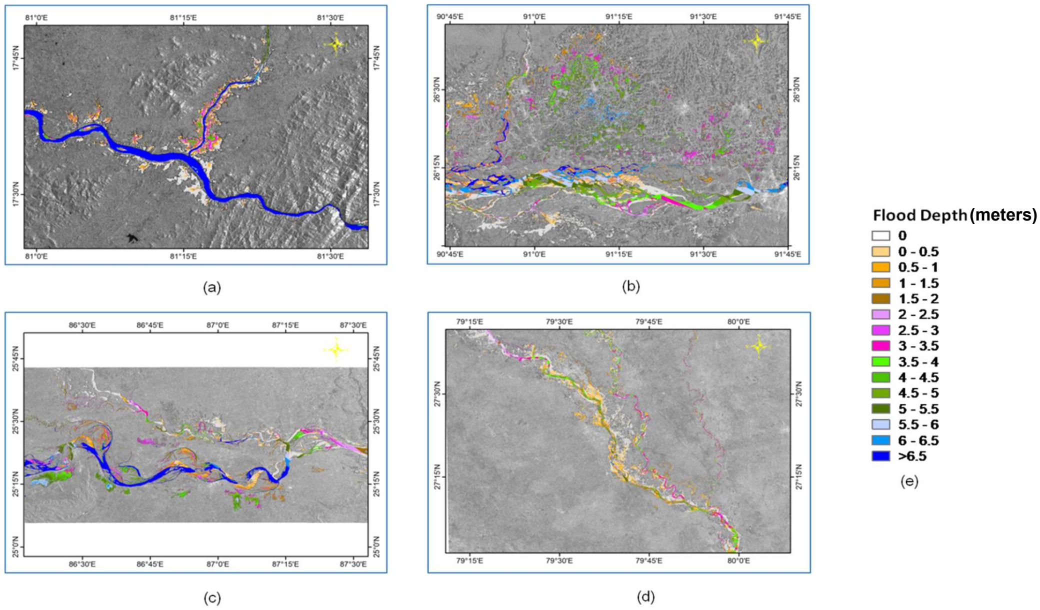

Figure:8: Flood depths calibrated using STA Technique for (a)Andhra Pradesh (b)Assam (c)Bihar and (d) Uttar Pradesh States (e)Legend for the Flood depth in meters

4.2.3 Validation of results

The water levels that have been derived using Trend Surface Analysis (TSA) technique in four case study areas is compared against field-based water level measurements at gauge station provided by CWC on the same particular day and time. The below figure 9 describes the method of comparison between the field-based measurement and TSA output. At each CWC provided River gauge station, TSA interpolated water levels are computed. At that particular location, date and time, field measured Water level is taken as reference for comparison study. The below table 4 shows the comparison study. TSA interpolated water levels are also compared against Flood Water Depth Estimation (FWDET) method. Water level is calculated using FWDET method in Open Source QGIS environment by taking same study area's inundated water layer and DEM as input.

https://doi.org/10.5194/egusphere-2024-2278
Preprint. Discussion started: 25 October 2024

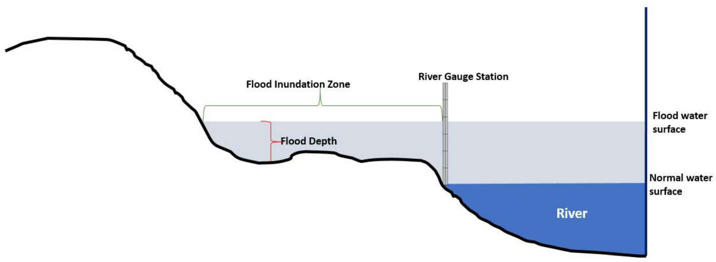

Figure 9: Pictorial representation of Flood plain and River Gauge station

S.No	Water Gauge Station Name	Field Measured Water Levels	TSA Interpolated Water Levels in meters	FWDET Interpolated Water Levels in meters
ANDHRA PRADESH				
1.	Kunavaram	41.02	40.63	46.62
2.	Koida	39.72	39.68	42.19
ASSAM				
1.	Beki Rd Bridge	44.92	46.4	41
2.	Pangladiya NT Road Xing	52.84	51.5	50.5
3.	Pandu	47.25	47.12	41.5
4.	Guwahathi	48.19	48.6	42
BIHAR				
1.	Baltara	34.9	34.08	32.85
2.	Kahalgaon	31.08	31.459	24
3.	Azamabad	30.54	30.16	24
4.	Kursela	29.98	28.98	27
UTTAR PRADESH				
1.	Dabri	137.18	138.6	136.21
2.	Fathegarh	137.78	137.4	136.05
3.	Kannauj	125.67	126	125.82
4.	Bewar	138.32	139.04	150.3

345 **Table 4:** Comparison study of Water levels among between field measurements, TSA and FWDET

https://doi.org/10.5194/egusphere-2024-2278
Preprint. Discussion started: 25 October 2024

Water levels obtained from Trend Surface Analysis (TSA) Technique can be comparable to measurement at corresponding gauge stations as both follows the same ellipsoid for projection ie WGS 84 and for both measurements, water levels are measured from Mean sea level (M.S. L). As LIDAR DEM is available in Godavari Flood plain, this DEM is taken as reference for calculation of water levels using TSA and FWDET Method. For remaining study areas, COPERNICUS FABDEM is taken as input. The results of the flood water surface derived from surface trend analysis and the Flood Water Depth Estimation Tool (FWDET) indicate that the water surface from the trend analysis closely matches the CWC water surface at gauge stations, whereas the surface derived from the FWDET tool shows significant deviations. Around TSA estimates deviate from a field level measurements floodwater depth estimation by <65cms on an average of 14 gauge stations. Most of interpolated water levels has small difference (<0.5m) with field measurements. The most underestimation of water levels by TSA method is due to the presence of real time gauge station in the upstream flood plain. Similarly, overestimation of water levels is due to presence of gauge station in downstream flood plain. Trend surface methods offer a more balanced and accurate representation of the flood surface in such cases. However, it is observed that slope of the flood affected area plays a major role in flood depth efficiency. For Gentle slope surfaces, the accuracy of this method is better.

Graphs are plotted as per figure 10 for the case studies against River gauge station water level and Field measurement, TSA and FWDET methods. In all the case studies, Trend Surface Analysis method outperforms FwDET when compare to field measurements. Root Mean Square Error (RMSE) is calculated for these two techniques. It is observed RMSE for TSA technique is 0.805 whereas FwDET is 5.23. Generally sharp transitions are observed in FwDET estimated depth, but here TSA provides the smoother distribution of depth map. As the estimated depths from TSA technique also depend on flood extent accuracy, from the above results it is understood that flood mapped output from Automatic Tile based segmentation is seemed to be accurate. The entire runtime for this automated python code ie Flood mapping and Flood depth has took around 2 min to 5 min depending on the area of case study on a desktop computer 3.2GHz processor and 128 GB RAM

https://doi.org/10.5194/egusphere-2024-2278
Preprint. Discussion started: 25 October 2024

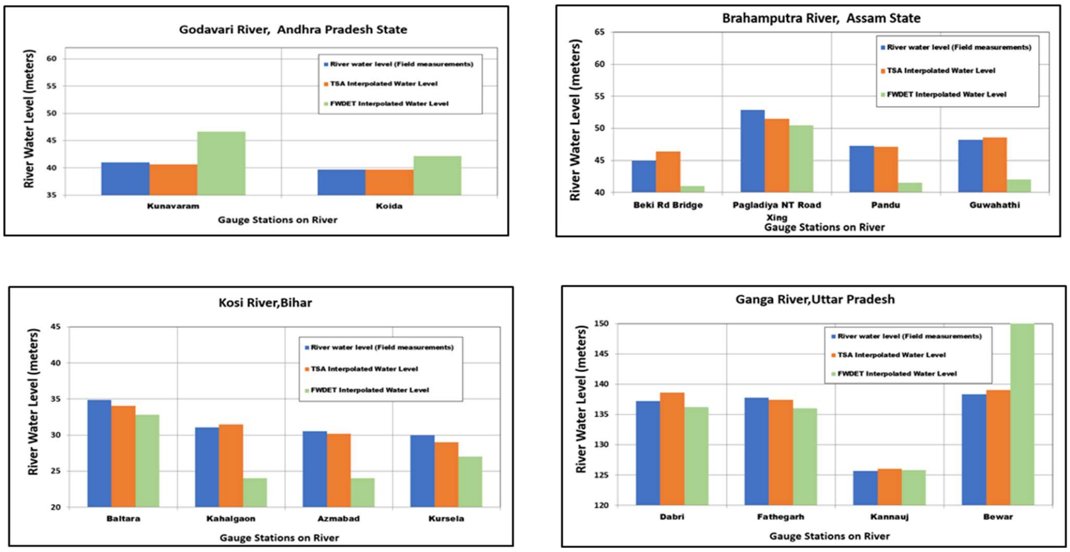

Figure:10 Comparison plots for water levels among field measured data, TSA and FWDET on all study areas

Conclusions

In summary, the Automatic Tile Based Classification Method applied to EOS-04 data, combined with the HAND (Height Above Nearest Drainage) tool, is highly effective for delineating flood layers, particularly in addressing hill shadows in SAR data to eliminate false water areas. Publicly available DEMs are valuable for plain areas with gentle slopes where high-resolution DEMs are not available for deriving flood depths, while steep flood-prone areas require fine-resolution DEMs for accurate flood depth estimation.

Adopting trend surface methods for interpolating water levels data allows for more accurate and reliable flood depth estimations in multi-dimensional river models. These methods capture the spatial trends inherent in river systems, providing better fitting and more precise representations of flood surfaces, especially in rapidly changing conditions. The Global Trend method is particularly effective for generating flood water surfaces in areas with extensive river flooding. This method fits a mathematical surface to the spatial data points, capturing underlying trends and offering a smoother and more accurate representation of the flood surface. By accounting for varying elevations and spatial trends present in the data, the global trend surface approach provides a comprehensive fitting that encompasses the overall spatial trend across the entire study area. This approach is especially useful in large river systems with complex flood behaviours. Combination of Automatic Tile based Segmentation technique and TSA technique are proven to be robust, accurate when validated against field measured data.

https://doi.org/10.5194/egusphere-2024-2278
Preprint. Discussion started: 25 October 2024

However, this method is greatly sensitive to DEM resolution and its appropriateness wrt flood layer. Sometimes manual control is required to align the DEM and corresponding flood layer. This method works well only for gentle slope areas. In Steep terrain areas Trend Surface Analysis may behave improperly.

Future research will focus on testing this tool on other parts of the country and try to improve the methodology based on terrain conditions.

Code and data availability

Nil.

Author contributions

Amani and Shashi developed this automated tool. Amani and Suresh tested this tool on field data. Amani, Suresh and Shashi contributed in paper writing. Durga Rao, Srinivas and Prakash technically guided and supported in this automation of Tool.

Competing interests

The authors declare that they have no conflict of interest.

References

Bazi, Y., Bruzzone, L., and Melgani, F.: An unsupervised approach based on the generalized Gaussian model to automatic change detection in multitemporal SAR images, IEEE Trans. Geosci. Remote Sens., 43, 2005.

Boni, G., Ferraris, L., Pulvirenti, L., Squicciarino, G., Pierdicca, N., Candela, L., Pisani, A. R., Zoffoli, S., Onori, R., Proietti, C., and Pagliara, P.: A prototype system for flood monitoring based on flood forecast combined with COSMO-SkyMed and Sentinel-1 data, IEEE J. Sel. Top. Appl. Earth Obs. Remote Sens., 9, 2794–2805, https://doi.org/10.1109/JSTARS.2016.2514402, 2016.

Bovolo, F. and Bruzzone, L.: A split-based approach to unsupervised change detection in large-size multitemporal images: application to tsunami-damage assessment, IEEE Trans. Geosci. Remote Sens., 45, 1658–1670, https://doi.org/10.1109/TGRS.2007.895413, 2007.

Cao, H., Zhang, H., Wang, C., and Zhang, B.: Operational flood detection using Sentinel-1 SAR data over large areas, Water, 11, 786, https://doi.org/10.3390/w11040786, 2019.

Chini, M., Hostache, R., Giustarini, L., and Matgen, P.: A hierarchical split-based approach for parametric thresholding of SAR images: flood inundation as a test case, IEEE Trans. Geosci. Remote Sens., 55, 6975–6988, https://doi.org/10.1109/TGRS.2017.2740462, 2017.

Chini, M., Pelich, R., Pulvirenti, L., Pierdicca, N., Hostache, R., and Matgen, P.: Sentinel-1 InSAR coherence to detect floodwater in urban areas: Houston and Hurricane Harvey as a test case, Remote Sens., 11, 107–120, https://doi.org/10.3390/rs11020107, 2019.

Chorley, R. J., and Haggett, P.: Trend surface mapping in geographical research, Trans. Inst. Br. Geogr., 37, 47–67, https://doi.org/10.2307/621128, 1965.

Cohen, S., Brakenridge, G. R., Kettner, A., Bates, B., Nelson, J. M., McDonald, R. R., Huang, Y.-F., Munasinghe, D., and Zhang, J.: Estimating floodwater depths from flood inundation maps and topography, J. Am. Water Resour. Assoc., 2009.

Cohen, S., Peter, B. G., Haag, A., Munasinghe, D., Moragoda, N., Narayanan, A., and May, S.: Sensitivity of remote sensing floodwater depth calculation to boundary filtering and digital elevation model selections, Am. Water Resour. Assoc., 2022.

Costabile, P., Costanzo, C., Ferraro, D., and Barca, P.: Is HEC-RAS 2D accurate enough for storm-event hazard assessment? Lessons learnt from a benchmarking study based on rain-on-grid modelling, J. Hydrol., 2021.

Elkhrachy, I.: Flash flood water depth estimation using SAR images, digital elevation models, and machine learning algorithms, Remote Sens., 14, 440, https://doi.org/10.3390/rs14030440, 2022.

Giacomelli, A., Mancini, M., and Rosso, R.: Assessment of flooded areas from ERS-1 PRI data: an application to the 1994 flood in Northern Italy, Phys. Chem. Earth, 20, 469–474, https://doi.org/10.1016/S0079-1946(96)00009-6, 1995.

Giustarini, L., Hostache, R., and D.K.O., G.: Probabilistic flood mapping using synthetic aperture radar data, IEEE Trans. Geosci. Remote Sens., 54, 6958–6969, https://doi.org/10.1109/TGRS.2016.2592951, 2016.

Greifeneder, F., Wagner, W., Sabel, D., and Naeimi, V.: Suitability of SAR imagery for automatic flood mapping in the Lower Mekong Basin, Int. J. Remote Sens., 35, 2857–2874, https://doi.org/10.1080/01431161.2014.880829, 2014.

Horritt, M. S., Mason, D. C., and Luckman, A. J.: Flood boundary delineation from Synthetic Aperture Radar imagery using a statistical active contour model, Int. J. Remote Sens., 22, 2489–2507, 2001.

Islam, M. M., and Sadu, K.: Flood damage and modelling using satellite remote sensing data with GIS: Case study of Bangladesh, in: Remote Sensing and Hydrology 2000, IAHS Publication, edited by: Owe, M., Brubaker, K., Ritchie, J., and Rango, A., Oxford, UK, 455–458, 2001.

Joshi, A., Agrawal, S., and Singh, R. P.: Potential of EOS-4 imagery for SAR interferometry, Remote Sens. Appl. Soc. Environ., 32, 101010, https://doi.org/10.1016/j.rsase.2023.101010, 2023.

Kittler, J., and Illingworth, J.: Minimum error thresholding, Pattern Recognit., 19, 41–47, https://doi.org/10.1016/0031-3203(86)90030-0, 1986.

Kuenzer, C., Guo, H., Schlegel, I., Tuan, V., Li, X., and Dech, S.: Varying scale and capability of Envisat ASAR-WSM, TerraSAR-X Scansar and TerraSAR-X Stripmap data to assess urban flood situations: a case study of the Mekong delta in Can Tho province, Remote Sens., 5, 5122–5142, https://doi.org/10.3390/rs5105122, 2013.

Lam, N. S.-N.: Spatial interpolation methods: a review, The Am. Cartogr., March 2013.

https://doi.org/10.5194/egusphere-2024-2278
Preprint. Discussion started: 25 October 2024

Li, N., Wang, R., Liu, Y., Du, K., Chen, J., and Deng, Y.: Robust river boundaries extraction of dammed lakes in mountain areas after Wenchuan Earthquake from high-resolution SAR images combining local connectivity and ACM, ISPRS J. Photogramm. Remote Sens., 94, 91–101, 2014.

Manjusree, P., Kumar, L. P., Bhatt, C. M., Rao, G. S., and Bhanumurthy, V.: Optimization of threshold ranges for rapid flood inundation mapping by evaluating backscatter profiles of high incidence angle SAR images, Int. J. Disaster Risk Sci., 3, 113–122, 2012.

Mason, D. C., Giustarini, L., Garcia-Pintado, J., and Cloke, H. L.: Detection of flooded urban areas in high-resolution synthetic aperture radar images using double scattering, Int. J. Appl. Earth Obs. Geoinf., 28, 150–159, https://doi.org/10.1016/j.jag.2013.12.002, 2014.

Mason, D. C., Speck, R., Devereux, B., Schumann, G. J. P., Neal, J. C., and Bates, P. D.: Flood detection in urban areas using TerraSAR-X, IEEE Trans. Geosci. Remote Sens., 48, 2010.

Marti-Cardona, B., Dolz-Ripolles, J., and Lopez-Martinez, C.: Wetland inundation monitoring by the synergistic use of ENVISAT/ASAR imagery and ancillary spatial data, Remote Sens. Environ., 139, 171–184, https://doi.org/10.1016/j.rse.2013.08.020, 2013.

Martinis, S., Kersten, J., and Twele, A.: A fully automated TerraSAR-X based flood service, ISPRS J. Photogramm. Remote Sens., 104, 203–212, https://doi.org/10.1016/j.isprsjprs.2014.07.014, 2015.

Martinis, S., Twele, A., Strobl, C., Kersten, J., and Stein, E.: A multi-scale flood monitoring system based on fully automatic MODIS and TerraSAR-X processing chains, Remote Sens., 5, 5598–5619, 2013.

Mazzarino, M., and Bonifazi, A.: A new approach to flood mapping from SAR images based on the analysis of water-to-land transitions, Int. J. Remote Sens., 39, 2233–2255, https://doi.org/10.1080/01431161.2017.1415867, 2018.

Mehr, A. J., Nejadkoorki, F., and Makhdoum, M. M.: Assessing the capabilities of C-band SAR data for flood mapping: a case study of the 2010 floods in Pakistan, Remote Sens. Environ., 119, 238–247, https://doi.org/10.1016/j.rse.2011.12.013, 2012.

Nemani, R. R., and Running, S. W.: Estimation of global land surface evaporation using satellite data, J. Appl. Meteorol. Climatol., 34, 1395–1409, 1995.

Nuth, C., and Kääb, A.: Two decades of multiview stereo topographic mapping of the Earth's surface, Remote Sens. Environ., 169, 54–65, https://doi.org/10.1016/j.rse.2015.08.023, 2015.

Pender, G., and Chanson, H.: The analysis of high-resolution floodplain inundation and flood risk using a remote sensing approach, Water, 10, 163, https://doi.org/10.3390/w10020163, 2018.

Perciavalle, V., Bagnato, S., and Lupo, D.: The use of SAR images for flood monitoring in Sicilian coastal areas: first results of an experimental study, Remote Sens., 12, 1536, https://doi.org/10.3390/rs12091536, 2020.

Platt, S. R., and Tazik, D. J.: Use of remote sensing in flood prediction: lessons from the 1998 flooding of the Red River in North Dakota and Minnesota, Water Resour. Bull., 34, 289–300, 1998.

https://doi.org/10.5194/egusphere-2024-2278
Preprint. Discussion started: 25 October 2024

Pulselli, F. M., and Salata, F.: Flood inundation mapping from optical remote sensing images and its operational integration with local emergency management protocols, Nat. Hazards Earth Syst. Sci., 16, 1357–1372, https://doi.org/10.5194/nhess-16-1357-2016, 2016.

Schumann, G., Bates, P. D., Horritt, M. S., Matgen, P., and Pappenberger, F.: Progress in integration of remote sensing–derived flood extent and stage data and hydraulic models, Rev. Geophys., 47, https://doi.org/10.1029/2008RG000274, 2009.

Scolobig, A., and Petrucci, O.: The role of imagery in building flood resilience: a case study from the 2014 flood in the Emilia-Romagna region, Italy, Nat. Hazards Earth Syst. Sci., 16, 1549–1563, https://doi.org/10.5194/nhess-16-1549-2016, 2016.

Stewart, C., and Arnold, M.: Flood risk assessment and management in a changing climate: new approaches and solutions, Water, 11, 56, https://doi.org/10.3390/w11010056, 2019.

Tabrizi, S. J. and Rahimi, M. M.: A novel model for flood mapping using multispectral remote sensing images, Remote Sens., 13, 2120, https://doi.org/10.3390/rs13122120, 2021.

Van Zyl, J. J., and Jezek, K. C.: A remote sensing approach to flood assessment and mapping, Remote Sens. Environ., 119, 134–147, https://doi.org/10.1016/j.rse.2011.02.012, 2012.

Voigt, S., and Rinnert, E.: A concept for rapid flood mapping using synthetic aperture radar data based on the normalised water index, Remote Sens., 10, 1037, https://doi.org/10.3390/rs10071037, 2018.

Wong, H. K., Chan, T. O., and Cheung, M. K.: Real-time flood monitoring system based on near real-time data acquisition and satellite remote sensing, IEEE J. Sel. Top. Appl. Earth Obs. Remote Sens., 9, 1320–1329, https://doi.org/10.1109/JSTARS.2016.2530861, 2016.

Xu, H., and Lin, H.: Use of SAR data for urban flood mapping, Remote Sens. Environ., 143, 147–160, https://doi.org/10.1016/j.rse.2013.02.013, 2013.